Exosome-derived microRNA-433 inhibits tumorigenesis through incremental infiltration of CD4 and CD8 cells in non-small cell lung cancer

BOYANG LIU[1], RUIPING ZHANG[2], YUNGANG ZHU[3] and RUISHENG HAO[1]

Departments of [1]Radiation and [2]Radiation Oncology, Tianjin Medical University Cancer Institute and Hospital, National Clinical Research Center of Cancer, Key Laboratory of Cancer Prevention and Therapy, Tianjin's Clinical Research Center for Cancer, Tianjin 300060; [3]Department of Radiation Oncology, Tianjin Teda Hospital, Tianjin 300457, P.R. China

Received August 3, 2020; Accepted April 22, 2021

DOI: 10.3892/ol.2021.12868

Abstract. Tumor-derived exosomal microRNAs (miRNAs/miRs) serve a vital biological role in tumorigenesis and development, but the effects and underlying mechanisms remain unclear. To explore the impact of exosomal miR-433 in non-small cell lung cancer (NSCLC) and understand its mechanism of action in NSCLC progression, the present study isolated the exosomes from the plasma of patients with NSCLC after chemotherapy and found that miR-433 expression was lower in plasma of patients with resistant NSCLC compared with in plasma of patients with sensitive NSCLC and in normal serum. Additionally, miR-433 expression was markedly negatively associated with a large tumor size, distant metastasis, advanced TNM stage and a poor prognosis in patients with NSCLC. miR-433 inhibited tumor growth by blocking the cell cycle *in vitro* and *in vivo*, as well as by promoting apoptosis and T-cell infiltration in the tumor microenvironment. Additionally, miR-433 inhibited chemoresistance to cisplatin by regulating DNA damage. Moreover, miR-433 inactivated the WNT/β-catenin signaling pathway by targeting transmembrane p24 trafficking protein 5 in NSCLC. Overall, the current findings may provide a potential prognostic biomarker and therapeutic target for patients with NSCLC.

Introduction

Lung cancer is one of the most frequently diagnosed types of cancer in both men and women worldwide; ~1.8 million new people were diagnosed in 2012, with 1.6 million fatalities (1). It is estimated that the United States alone had >230,000 new cases in 2018 (1). Lung cancer is a very heterogeneous disease at a cellular and histological level. It is well known that 80-85% of lung cancer cases are classified as non-small cell lung cancer (NSCLC), which includes several subtypes, including undifferentiated carcinoma or large cell carcinoma, squamous cell carcinoma, adenocarcinoma and other subtypes (2). The average 5-year overall survival rate for patients with lung cancer is 18% due to the advanced stages of disease diagnosed and its known heterogeneity, including tumor microenvironmental factors, complex molecular characteristics and the limited therapy options (3). New therapeutic strategies are emerging with the introduction of several lines of tyrosine kinase inhibitors in patients with ALK, EGFR, NTRK and ROS1 mutations (4). In addition, immune checkpoint inhibitors have markedly improved the NSCLC treatment (5). However, there are increasing problems, such as optimal patient selection, optimal duration of treatment and clinical implications of combined treatments, that limit its discriminatory potency. Therefore, it is important to identify the molecular mechanisms responsible for the pathogenesis of NSCLC.

Exosomal RNA is involved in biological processes in tumor cells, immune cells and stromal cells (6). A diverse collection of the exosomal RNA species has been identified by RNA sequencing analysis, and microRNAs (miRNAs/miRs) are the most abundant in extracellular vesicles (7). miRNAs, a group of small non-coding RNAs (18-22 bp), negatively regulate the expression of target genes by reducing the stability of the target mRNA or post-transcriptionally inhibiting the translation process (8). Exosomal miRNAs serve important roles in proliferation, invasion, metastasis and drug resistance by regulating gene expression in target cells (9,10). In addition, numerous studies have revealed that downregulation or upregulation of miRNAs is associated with the initiation and development of cancer, and that miRNAs can act as either an oncogene or a tumor suppressor gene (11,12). For example, Han *et al* (13) has reported that exosomal miR-26b-5p decreases activating transcription factor 2 expression to enhance the radiosensitivity of X-radiation in lung adenocarcinoma cells. Wang *et al* (14) has reported that miR-23b inhibits cell proliferation, invasion and migration by downregulating RUNX family transcription factor 2 through the

Correspondence to: Professor Ruisheng Hao, Department of Radiation, Tianjin Medical University Cancer Institute and Hospital, National Clinical Research Center of Cancer, Key Laboratory of Cancer Prevention and Therapy, Tianjin's Clinical Research Center for Cancer, 5 Huanhu West Road, Hexi, Tianjin 300060, P.R. China
E-mail: boyang_tjtumor@163.com

Key words: exosome, microRNA-433, transmembrane p24 trafficking protein 5, non-small cell lung cancer, T-cell infiltration, Wnt/β-catenin

Wnt/β-catenin signaling pathway in NSCLC. miR-433 expression has been shown to be downregulated in glioma (15), cervical cancer (16), colorectal cancer (17), breast cancer (18), esophageal squamous cell carcinoma (ESCC) (19) and oral squamous cell carcinoma (20), among others. Previously, Liu *et al* (21) and Li *et al* (22) have reported that miR-433 decreases cell proliferation and invasion, as well as tumor progression in NSCLC (21,22). However, the characteristic molecular mechanism and the underlying role of miR-433 require further investigation, especially in the tumor microenvironment of NSCLC.

In the present study, exosomes were isolated from the plasma of patients with NSCLC after the combined chemotherapy of gemcitabine and cisplatin treatment, and miR-433 expression was analyzed in the plasma of patients with resistant NSCLC, patients with sensitive NSCLC and in normal serum. However, the exact function and underlying mechanism of miR-433 in NSCLC remains unclear. Therefore, the present study was performed to investigate the effects of miR-433 on NSCLC cell proliferation, apoptosis, DNA damage and tumor growth *in vivo*.

Materials and methods

Collection of NSCLC tissues. A total of 50 NSCLC tissues and adjacent normal lung tissues (2 cm away from the tumor edge) from patients (n=50; median age, 59 years; age range, 29-83 years; 16 females and 34 males) were collected between January 2018 and January 2020. All patients were pathologically diagnosed and underwent therapeutic surgery at the Tianjin Medical University Cancer Institute and Hospital (Tianjin, China). Serum samples (4 ml) were collected from patients diagnosed with NSCLC (n=33; 18 chemotherapy-resistant patients and 15 chemotherapy-sensitive patients) and healthy individuals (n=19; median age, 46 years; age range, 25-19 years; 9 females and 10 males). The current study was conducted under the International Ethical Guidelines for Biomedical Research Involving Human Subjects with the approval of the Ethics Committee of Tianjin Medical University Cancer Institute and Hospital and carried out in accordance with the Declaration of Helsinki (approval no. EK2019034), and all participants gave their written informed consent.

Cell culture and transfection. A549, H1299 and LLC cells were purchased from iCell Bioscience, Inc., and were cultured in DMEM (Invitrogen; Thermo Fisher Scientific, Inc.) with 10% FBS (Gibco; Thermo Fisher Scientific, Inc.), 100 μg/ml streptomycin and 100 U/ml penicillin (both Beyotime Institute of Biotechnology) at 37˚C in 5% CO_2. Briefly, once cells reached 70-80% confluence, antisense oligonucleotide (ASO)-miR-433 (100 nM; 5'-ACACCGAGGAGCCCAUCA UGAU-3'; Shanghai GenePharma Co., Ltd.), pri-miR-433 (2 μg; Shanghai GenePharma Co., Ltd.) or pTMED5 (2 μg; Shanghai GenePharma Co., Ltd.) were transfected into A549 and H1299 cells using Lipofectamine® 2000 (Invitrogen; Thermo Fisher Scientific, Inc.) according to the manufacturer's instructions. As non-targeting negative controls (NCs), ASO-NC (100 nM; 5'-CAGUACUUUUGUGUAGUACAA-3'; Shanghai GenePharma Co., Ltd.) for the ASO-miR-433 or the empty vector pcDNA3 for pri-miR-433 and pTMED5 (2 μg; Shanghai GenePharma Co., Ltd.) were also transfected into A549 and H1299 cells. The cells were incubated for 6 h at 37˚C. Subsequently, the transfection medium was replaced with complete medium containing 10% FBS. After 48 h at 37˚C, cells were collected for subsequent analyses. Recombinant lentiviruses expressing lenti-miR-433 or the empty lentiviral vector pLENT-Puro-MIR-GFP were produced by Shanghai GeneChem Co., Ltd. A total of $6x10^5$ LLC cells were infected with concentrated lentivirus (MOI=40) in the presence of 8 μg/ml polybrene (Sigma Aldrich; Merck KGaA). After 60 h of incubation at 37˚C, cells were selected using puromycin (3 μg/ml; Sigma Aldrich; Merck KGaA) for 5 days before subsequent experiments.

Isolation of exosomes from serum. Exosome fractions were prepared using the exoEasy Maxi kit (Qiagen China Co., Ltd.) according to the manufacturer's instructions.

Reverse transcription-quantitative (RT-qPCR). Total RNA was extracted from tissues and A549 and H1299 cells using TRIzol® Reagent (Invitrogen; Thermo Fisher Scientific, Inc.). RT was performed using the RT-PCR Quick Master Mix kit (Toyobo Life Science) according to the manufacturer's protocol. The resultant cDNA was amplified by qPCR using the following primers: miR-433 forward, 5'-TCGGCAATCATG ATGGGCTCCTC-3' and reverse, 5'-CTCAACTGGTGTCGT GGAGTC-3'; U6 forward, 5'-CTCGCTTCGGCAGCACA-3' and reverse, 5'-AACGCTTCACGAATTTGCGT-3'; TMED5 forward, 5'-CCTTTCTACCCTTGATTT-3' and reverse, 5' -TATAGCCACATTCTCCTT-3'; β-actin forward, 5'-CGT GACATTAAGGAGAAGCTG-3' and reverse, 5'-CTAGAA GCATTTGCGGTGGAC-3'. Amplification and detection were performed with a SYBR-Green PCR kit (Applied Biosystems; Thermo Fisher Scientific, Inc.) for TMED5 and β-actin, and SYBR® Green Realtime PCR Master Mix (Toyobo Life Science) for miR-433 and U6 on the ABI PRISM 7700 Sequence Detection System (Applied Biosystems; Thermo Fisher Scientific, Inc.). The thermocycling conditions were as follows: 95˚C for 4 min, followed by 40 cycles of 95˚C for 30 sec, 59˚C for 30 sec and 72˚C for 1 min, with a final extension at 72˚C for 5 min. The relative expression levels were normalized to the endogenous controls U6 for miR-433 and β-actin for TMED5, and were expressed using the $2^{-\Delta\Delta Cq}$ method (23).

Western blotting. The exosomes were mixed with 1X SDS loading buffer and A549 and H1299 cells were washed in cold 1X PBS and lysed using RIPA lysis buffer (Beyotime Institute of Biotechnology) supplemented with a protease phosphatase inhibitor, boiled at 95˚C for 5 min and centrifuged in 12,000 x g for 5 min at 4˚C. Protein concentration was determined using the BCA Protein Assay kit (Beyotime Institute of Biotechnology). Proteins in supernatants (30 μg/lane) were separated via 10% SDS-PAGE and transferred onto PVDF membranes (EMD Millipore), which were blocked with 5% skimmed milk (Solarbio Science & Technology Co., Ltd.) for 1 h at room temperature. Subsequently, the membranes were incubated overnight at 4˚C with primary antibodies against CD63 (cat. no. ab213090; 1:1,000), Alix (cat. no. ab225555; 1:2,000), tumor susceptibility 101 (TSG101; cat. no. ab125011; 1:2000), cleaved caspase3 (cat. no. ab49822; 1:600), cleaved poly(ADP-ribose)polymerase (PARP; cat. no. ab32064; 1:5,000), tumor protein p53 binding protein 1 (53BP1;

cat. no. ab175188; 1:5,000), H2AX (cat. no. ab124781; 1:3,000), phosphorylated (p)-β-catenin (cat. no. ab75777; 1:1,000), β-catenin (cat. no. ab68183; 1:3,000), c-myc (cat. no. ab32072; 1:2,000), cyclin D1 (cat. no. ab16663; 1:1,000), TMED5 (cat. no. ab228920; 1:2,000) and GAPDH (cat. no. ab8245; 1:5,000) (all from Abcam). After washing, protein samples were incubated with HRP-conjugated secondary antibodies (cat. no. ab6789; 1:3,000; Abcam) for 1 h at room temperature. Finally, an ECL kit (Beyotime Institute of Biotechnology) was used to assess protein bands. The data were analyzed via densitometry using ImageJ software (version 1.8.0; National Institutes of Health) and normalized to the expression of the internal control GAPDH.

Flow cytometry assay for cell cycle and apoptosis analysis. For the analysis of cell cycle, the cells were digested using trypsin (Invitrogen; Thermo Fisher Scientific, Inc.) and stained with PI (Beyotime Institute of Biotechnology) using a Cycletest™ Plus DNA Reagent kit (BD Biosciences) according to the manufacturer's manual, and cells were detected by flow cytometry assay. Briefly, a total of $2x10^6$ cells/well were seeded onto 6-well plates. On the next day, A549 and H1299 cells were harvested and fixed in 70% ethanol at 4˚C overnight. The fixed cells were then incubated with PBS containing 0.1% Triton X-100 for 30 min at room temperature, and then stained with 20 μg/ml PI for 30 min in the dark at room temperature. The stained cells were analyzed using the NovoCyte flow cytometer with the NovoCyte 1.4.1 software (both ACEA Biosciences, Inc.; Agilent Technologies, Inc.). The proliferation index (PI) was calculated according to the following formula: $PI=(S + G_2/M)/(G_0/G_1 + S+ G_2/M)$.

Apoptosis was detected using an Annexin V-FITC kit (Solarbio Science & Technology Co., Ltd.) according to the manufacturer's protocol. Briefly, A549 and H1299 cells were washed three times with PBS and then fixed with 100 μl binding buffer (Solarbio Science & Technology Co., Ltd.). Subsequently, 5 μl PI and 5 μl Annexin V-FITC were used to stain the cells for 15 min in the dark at room temperature. Finally, cells were analyzed with a flow cytometer (Epics XL; Beckman Coulter, Inc.) and FlowJo software (v.10.4.2; FlowJo LLC).

Cell Counting Kit-8 (CCK-8) assay. Briefly, A549 and H1299 cells were plated into the 96-well culture plates at a density of $3x10^3$ cells/well in 100 μl culture medium one day prior to transfection. At 0 and 48 h of culture, 10 μl CCK-8 reagent (Solarbio Science & Technology Co., Ltd.) was added into each well and incubated at 37˚C for 2 h. In addition, A549 and H1299 cells were plated into the 96-well culture plates at a density of $3x10^3$ cells/well in 100 μl culture medium one day prior to transfection with pcDNA and miR-433, and 1, 2, 3 or 4 μg/ml cisplatin (Solarbio Science & Technology Co., Ltd.) was added at 37˚C for 24 h. Relative cell proliferating rate was measured using a microplate reader (Thermo Fisher Scientific, Inc.) at an absorbance of 450 nm.

Colony formation assay. Following transfection with the pri-miR-433, ASO-miR-433, pTMED5 and the control group, NSCLC cells were seeded into 12-well culture dishes at a density of 500 cells/dish and cultured in a 5% CO_2 incubator at 37˚C. The medium was replaced every 3 days. After 14 days, cells were stained using 1% crystal violet at room temperature for 15 min (Beyotime Institute of Biotechnology).

In vivo experiments. A total of 10 6-week-old male C57BL/6J mice (20±2 g; 6-8 weeks old) were purchased from Beijing Vital River Laboratory Animal Technologies Co., Ltd. All mice were housed under a fixed 12-h light-dark cycle in a laminar flow room at constant temperature (23˚C) and humidity (40-70%), with ad libitum access to sterilized food and water. The mice were randomly divided into 2 groups (5 mice/group): Lenti-Con and Lenti-miR-433. Lentiviral-transduced LLC cells were resuspended in PBS and subcutaneously injected into the ventral forearm of mice. The behavior of mice and changes in body weight were recorded daily. During 1-4 week of *in vivo* explant assay, the subcutaneous lengths and widths of tumors were measured weekly. Mice were sacrificed 30 days post-injection, and the tumors were extracted and visually compared. The mice were euthanized using carbon dioxide (at a range rate of 30-70% of the chamber volume per minute), and their deaths were verified by checking eye color and reflex action. Tumor volume was calculated using the equation: $V = (LxW^2)/2$, where V represents the tumor volume, L represents the length and W represents the width. The study was approved by the Institutional Animal Care and Use Committee of Tianjin Medical University Cancer Institute and Hospital (approval no. LLSP2019017).

Immunohistochemistry (IHC). For IHC assays, tumor tissues were fixed with 4% formalin for 24 h at room temperature, paraffin-embedded and cut into 4-μm-thick sections. Subsequently, the slides were deparaffinized in xylene and rehydrated through a descending ethanol series. Antigen retrieval was performed with citrate buffer in a microwave oven. Subsequently, slides were blocked with 3% hydrogen peroxidase in methanol and 10% goat serum (Solarbio Science & Technology Co., Ltd.) for 1 h at room temperature. Slides were incubated with CD4 (cat. no. ab183685; 1:1,000; Abcam), CD8 (cat. no. ab217344; 1:1,000; Abcam), TMED5 (cat. no. SRP08852; 1:1,1000; Tianjin Saier Biotechnology Co., Ltd.) and β-catenin antibodies (cat. no. ab223075; 1:1,000; Abcam) overnight at 4˚C and then with HRP-labeled goat anti-rabbit IgG (cat. no. ab6721; 1:2,000; Abcam) for 30 min at room temperature. The slides were stained with DAB (1:50) as the chromogen and counterstained with hematoxylin for 1 min at room temperature. Slides were evaluated using an optic Olympus BX51 microscope at light field (Olympus Corporation; magnification, x200) with a Micro-Publisher 3.3 RTV camera (Q Imaging Scientific & Industrial Camera; Teledyne Photometrics).

Transcriptome analysis. Global characterization of T cells in NSCLC by single-cell sequencing was used to analyze the immune cell infiltration for TMED5 (Global characterization of T cells in non-small cell lung cancer by single-cell sequencing; http://lung.cancer-pku.cn/index.php).

Bioinformatics analysis. The Cancer Genome Atlas (TCGA) portal (https://tcgadata.nci.nih.gov/tcga/) was used for the gene expression data of 233 patients with chemotherapy-sensitive NSCLC, 279 patients with chemotherapy-resistant NSCLC

and 59 normal samples. Gene Expression Profiling Interactive Analysis (GEPIA) database (http://gepia.cancer-pku.cn/) and StarBase V3.0 (http://starbase.sysu.edu.cn/) were used to analyze TMED5 expression in NSCLC. Kaplan-Meier Plotter (http://kmplot.com/analysis/) was used to analyze the overall survival of patients with NSCLC with high or low miR-433 expression (504 patients with lung adenocarcinoma and 472 patients with lung squamous cell carcinoma). The Human Protein Atlas (https://www.proteinatlas.org/) was used to analyze the overall survival of patients with NSCLC with high (n=557) or low (n=437) TMED5 expression.

EGFP fluorescent reporter assay. This assay was performed as previously described (24). A549 and H1299 cells were co-transfected with pri-miR-433 (0.5 μg) or ASO-miR-433 (100 nM) together with pcDNA3/EGFP-TMED5 3'-untranslated region (UTR) wild-type or mutated reporter plasmids (0.5 μg) using Lipofectamine® 2000 (Invitrogen; Thermo Fisher Scientific, Inc.) according to the manufacturer's instructions. pDsRed2-N1 (0.05 μg; Clontech Laboratories, Inc.) was used for normalization. After 48 h of transfection, cells were lysed and the intensity of EGFP and RFP fluorescence was determined using an F-4500 fluorescence spectrophotometer (Hitachi, Ltd.).

Comet assay. The evaluation of DNA damage was analyzed with the alkaline comet assay using the Reagent kit for Single Cell Gel Electrophoresis Assay (Trevigen, Inc.) according to the manufacturer's instructions. A549 and H1299 cells were seeded at a density of 10^5 cells/well in 12-well plates. Cells were treated with bersaldegenin-1,3,5-orthoacetate (Sigma-Aldrich; Merck KGaA) at a concentration of 1.0 μg/ml for 6 h and 10 μg/ml taxol (Solarbio Science & Technology Co., Ltd.), used to induce DNA damage, for 4 h at 37˚C. Subsequently, A549 and H1299 cells were collected by centrifugation at 500 x g for 5 min at 4˚C and combined with low melting agarose at a ratio of 1:10, and 50 μl cell suspension was spread onto the CometSlides (Invitrogen; Thermo Fisher Scientific, Inc.). Slides were immersed in the lysis solution for 1 h at 4˚C, after which they were placed in the alkaline unwinding solution (Trevigen, Inc.) for 1 h at 4˚C. Slides were placed in the electrophoresis slide tray and immersed in the alkaline electrophoresis solution in the CometAssay ES unit (Trevigen, Inc.). Slides were submitted to electrophoresis at 1 V/cm for 30 min. Following electrophoresis, slides were washed and then stained with DAPI (Invitrogen; Thermo Fisher Scientific, Inc.) for 30 min at room temperature. Slides were analyzed under a fluorescence microscope (magnification, x200, Nikon PCM-2000; Nikon Corporation).

Top/fop luciferase assay. To analyze β-catenin transcriptional activity, TOP-flash luciferase (plasmid 16558; Addgene, Inc.) and FOP luciferase (plasmid 16559; Addgene, Inc.) and the indicated plasmids (pcDNA3 + pcDNA3, pcDNA3 + miR-433, miR-433 + pTMED5) were transfected into A549 and H1299 cells using Lipofectamine 2000 according to the manufacturer's protocol. Luciferase activity was measured after 48 h using a Dual-Luciferase Reporter Assay kit (Promega Corporation) according to the manufacturer's protocol, and *Renilla* luciferase activity was used as an internal control.

Table I. Association of miR-433 expression with the clinicopathological features of 50 patients with non-small cell lung cancer.

		miR-433 expression		
Variable	No.	Low (n=31)	High (n=19)	P-value
Age, years				
<60	21	12	9	0.547
≥60	29	19	10	
Sex				
Male	34	22	12	0.566
Female	16	9	7	
Tumor size				
≥5 cm	30	22	8	0.043[a]
<5 cm	20	9	11	
TNM stage				
I-II	19	8	11	0.023[a]
III-IV	31	23	8	
Distant metastasis				
No	24	11	13	0.026[a]
Yes	26	20	6	
Histological type				
Squamous	28	16	12	0.425
Adenocarcinoma	22	15	7	

[a]P<0.05.

Transmission electron microscopy (TEM) analysis and exosome particle size detection. For TEM analysis, isolated exosomes were fixed with 4% paraformaldehyde at room temperature for 30 min and 4% glutaraldehyde in 0.1 M phosphate buffer (pH 7.4) and then placed on a carbon-coated copper grid and immersed in a 2% phosphotungstic acid solution for examination (JEM-1200EX; JEOL, Ltd.). For exosome particle size detection, a total of 1 ml filtered PBS was used to mix the exosome and was then stored on ice. A disposable clean sample cell was selected and wiped with dust-free paper to ensure that no particles adhered to the outer tube wall. The exosome solution was slowly injected to avoid air bubbles, slightly tilting the sample cell. The sample cell was sealed with a lid. The instrument operating procedure was followed using the Nanosight NS 300 system (NanoSight; Malvern Panalytical).

Statistical analysis. SPSS 19.0 (IBM Corp.) statistical software was used for data analysis and GraphPad Prism V (GraphPad Software, Inc.) was used for image editing. Measurement data were expressed as the mean ± SD and compared using the unpaired t-test. Differences among multiple groups were determined using one-way ANOVA with Tukey's post-hoc test. The survival data was analyzed using Kaplan-Meier curves with the log-rank test. The χ^2 test was used to analyze whether miR-433 expression was associated with clinicopathological characteristics. P<0.05 was considered to indicate a statistically significant difference.

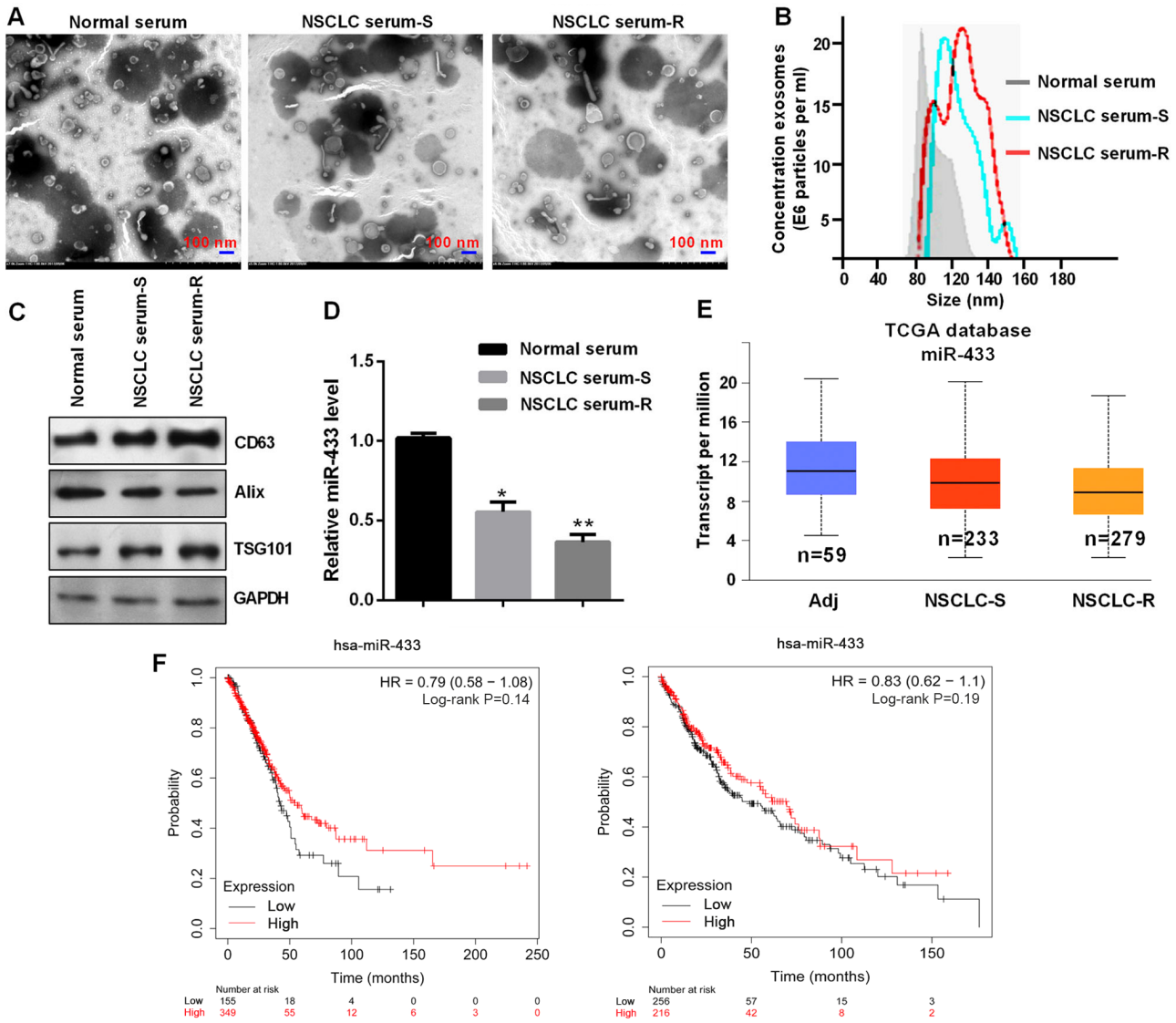

Figure 1. Exosome-derived miR-433 was downregulated. (A) Exosomes were assessed using transmission electron microscopy. Scale bar, 100 nm. (B) Western blot analysis of the exosomal markers CD63, Alix and TSG101. (C) Exosomes were detected by Nanosight particle tracking. (D) Reverse transcription-quantitative PCR of miR-433 expression in the indicated groups. *P<0.05 and **P<0.01 vs. normal serum. (E) TCGA database showed the miR-433 expression in the indicated groups. (F) Low expression levels of exosomal miR-433 predicted a poor prognosis in patients with NSCLC. Left panel, 504 patients with lung adenocarcinoma; right panel, 472 patients with lung squamous cell carcinoma. NSCLC, non-small cell lung cancer; S, sensitive; R, resistant; Adj, adjacent; miR, microRNA; TCGA, The Cancer Genome Atlas; HR, hazard ratio; TSG101, tumor susceptibility 101.

Results

Exosome-derived miR-433 expression is downregulated in NSCLC, especially in chemotherapy-resistant NSCLC. First, exosomes were isolated using the exoEasy Maxi kit from the serum of patients with NSCLC. Subsequently, TEM was used to verify the exosomal cup-shaped membranes (Fig. 1A). Nanosight particle tracking revealed that the sizes of these exosomes were ~80-150 nm (Fig. 1B). Western blot analysis confirmed the expression of specific exosomal markers such as CD63, Alix and TSG101 (Fig. 1C). miR-433 expression was lower in the serum of patients with chemotherapy-resistant NSCLC compared with that of patients with chemotherapy-sensitive NSCLC and with normal serum (Fig. 1D). miR-433 expression was negatively associated with a large tumor size, severe TNM stage and distant metastasis in patients with NSCLC (Table I). In addition, TCGA database showed lower miR-433 expression in patients with chemotherapy-resistant NSCLC (Fig. 1E). Furthermore, patients with NSCLC with low miR-433 expression exhibited a poor prognosis using Kaplan-Meier Plotter (Fig. 1F).

Suppressive role of miR-433 in NSCLC. To assess the role of miR-433 in NSCLC cells, gain-of-function and knockdown approaches were performed. RT-qPCR was used to confirm the transfection efficiency (Fig. 2A). As shown in Fig. 2B, CCK-8 assay indicated that miR-433 overexpression inhibited cell viability compared with the control group, while its inhibitor increased cell viability in H1299 and A549 cells (Fig. 2B). Similarly, pri-miR-433 and ASO-miR-433 significantly decreased or enhanced, respectively, the colony formation ability of A549 and H1299 cells compared with their respective control groups (Fig. 2C). Flow cytometry demonstrated that overexpression of miR-433 blocked cell

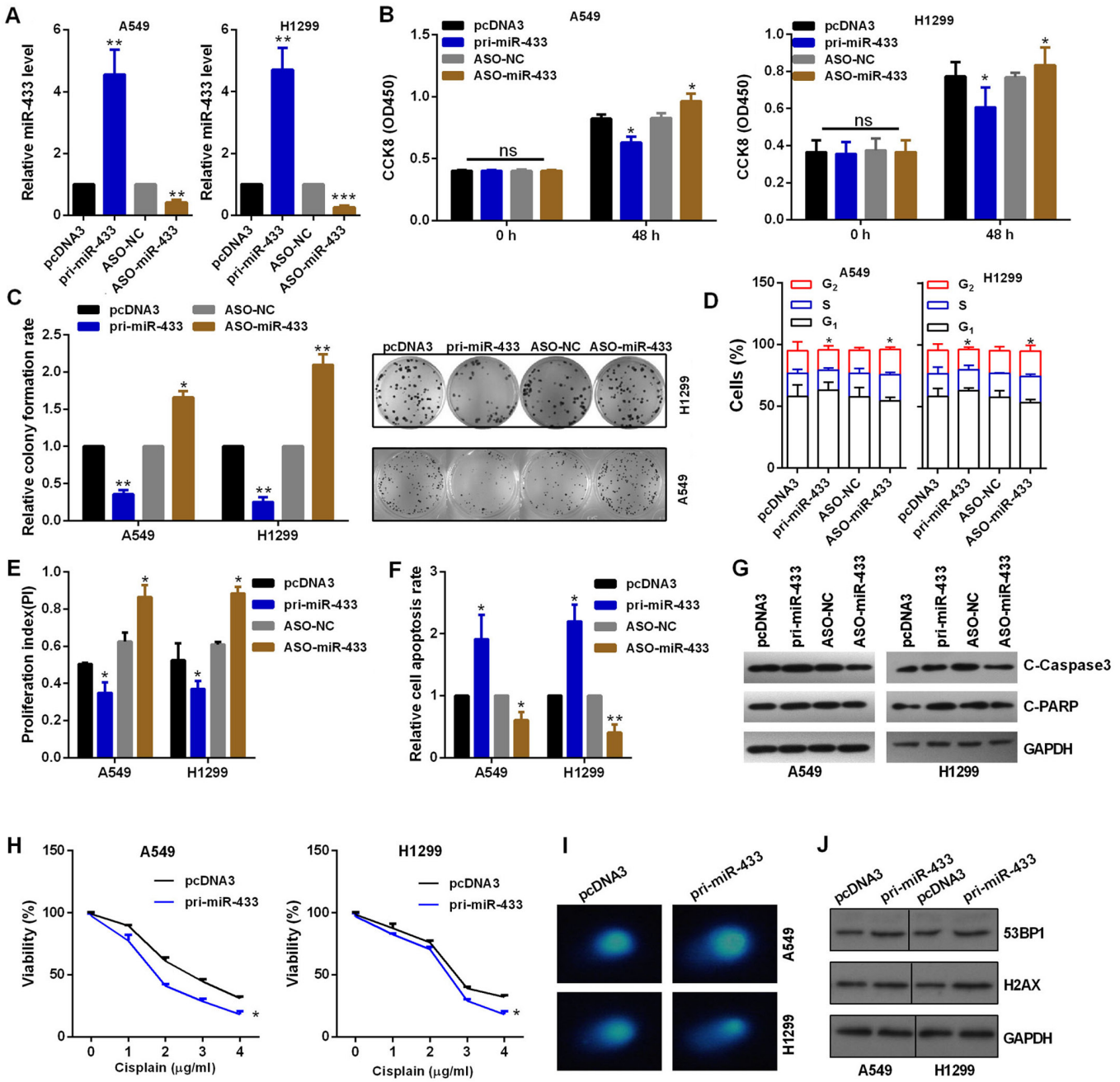

Figure 2. Suppressive role of miR-433 *in vitro*. (A) Efficiency of pri-miR-433 or ASO-miR-433 was detected by reverse transcription-quantitative PCR assay in A549 and H1299 cells. (B) Role of altered miR-433 expression on the viability of A549 and H1299 cells was detected by CCK-8 assay. (C) Colony formation assay showed the proliferation ability of cells transfected with pri-miR-433 or ASO-miR-433. (D) Flow cytometric analysis showed that miR-433 overexpression in A549 and H1299 cells resulted in an increase of cells in the G_0/G_1 phase and a decrease of cells in the S and G_2 phases. (E) miR-433 overexpression inhibited the PI, while miR-433-knockdown promoted the PI. (F) Flow cytometric assay showed miR-433 overexpression promoted apoptosis and ASO-miR-433 inhibited apoptosis in A549 and H1299 cells. (G) Western blot analysis showed the protein expression levels of C-caspase 3 and C-PARP in A549 and H1299 cells. (H) Transfected A549 and H1299 cells were treated with 0-4 μg/ml cisplatin in 96-well plates for 24 h. CCK-8 assay was then used to investigate cell viability. (I) Comet assays showed the degree of DNA breaks in A549 and H1299 cells transfected with the indicated plasmids treated with 10 μg/ml taxol for 4 h. (J) Western blot analysis showed the protein expression levels of 53BP1 and H2AX in A549 and H1299 cells transfected with the indicated plasmids treated with 10 μg/ml taxol for 4 h. *P<0.05, **P<0.01 and ***P<0.001 vs. pcDNA3 or ASO-NC. ns, not significant; CCK-8, Cell Counting Kit-8; OD, optical density; miR, microRNA; NC, negative control; ASO, antisense oligonucleotide; C, cleaved; PARP, poly(ADP-ribose)polymerase; 53BP1, tumor protein p53 binding protein 1; PI, proliferation index.

cycle progression, while miR-433-knockdown promoted cell cycle progression of A549 and H1299 cells by regulating the PI index (Figs. 2D and E, and S1A and B). Flow cytometry demonstrated that overexpression of miR-433 accelerated apoptosis in NSCLC cells (Figs. 2F and S1C and D), also demonstrated by the increased levels of cleaved caspase 3 and cleaved PARP (Fig. 2G). Knockdown of miR-433 inhibited apoptosis in NSCLC cells (Figs. 2F and S1C and D), also demonstrated by the decreased expression levels of cleaved caspase 3 and cleaved PARP (Fig. 2G). Subsequently, the effect of miR-433 on the regulation of chemoresistance to cisplatin was assessed. Cisplatin chemoresistance was

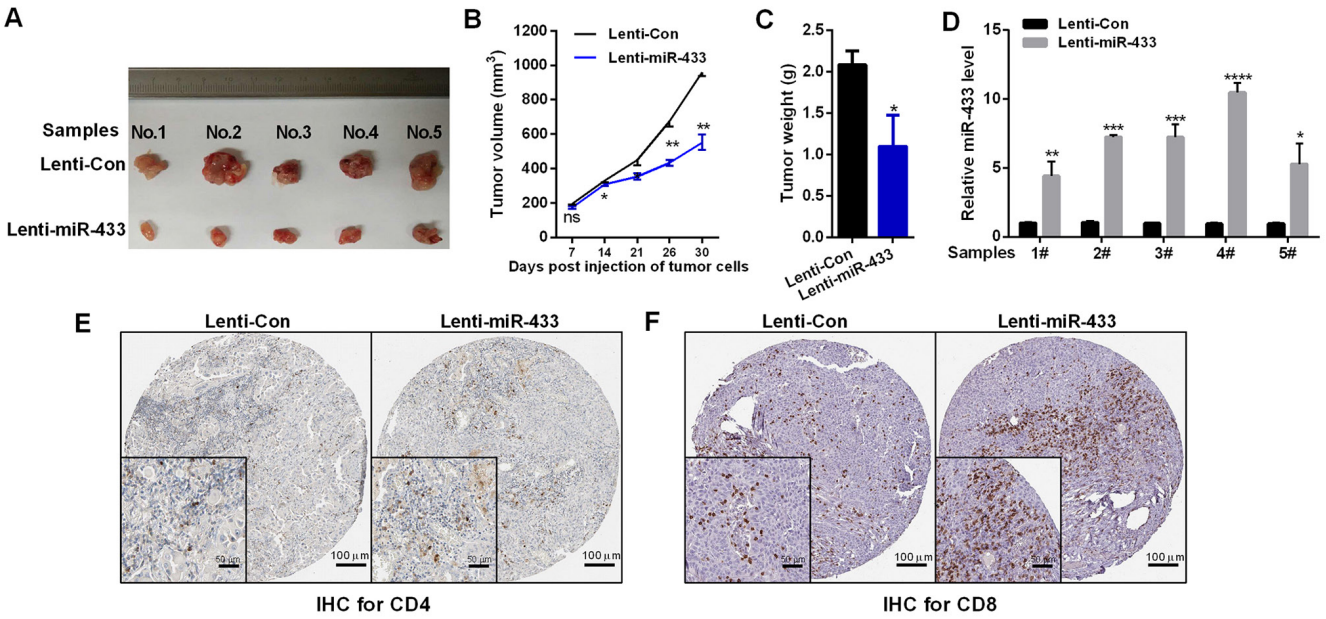

Figure 3. miR-433 inhibits tumor growth *in vivo*. Lenti-miR-433 inhibited (A) tumor size, (B) tumor volume and (C) tumor weight. (D) Reverse transcription-quantitative PCR of miR-433 expression in tumor tissues. IHC of (E) CD4 and (F) CD8 protein expression in tumor tissues. Scale bars, 50 and 100 μm. *P<0.05, **P<0.01, ***P<0.001 and ****P<0.0001 vs. Lenti-Con. ns, not significant; Lenti, lentivirus; Con, control; miR, microRNA; IHC, immunohistochemistry.

decreased when cells were treated with pri-miR-433 in A549 and H1299 cells compared with that in cells transduced with pcDNA3 in a dose-dependent manner with 0-4 μg/ml cisplatin, as assessed by CCK-8 assay (Fig. 2H). In addition, miR-433-overexpressing A549 and H1299 cells repaired DNA breaks more slowly than control vector-treated cells (Fig. 2I). Furthermore, miR-433 overexpression promoted the protein expression of 53BP1 or H2AX in A549 and H1299 cells (Fig. 2J).

miR-433 inhibits tumor growth by promoting CD4 and CD8 T-cell infiltration in vivo. To test whether miR-433 could enhance the antitumor effects of lung cancer, LLC cells were stably transfected with lenti-miR-433 or empty vector (lenti-Con). Mice injected with lenti-miR-433 exhibited decreased tumor volume and tumor weight compared with those injected with lenti-Con (Fig. 3A-C). The expression levels of miR-433 in tumors were confirmed by RT-qPCR assay (Fig. 3D). The effects of miR-433 on T-cell infiltration were evaluated, and it was found that miR-433 overexpression increased the CD4 and CD8 T-cell infiltration intratumorally, as assessed using IHC assay (Fig. 3E).

TMED5 is a direct target gene of miR-433. TMED5 was identified to have a binding site with miR-433 using StarBase V3.0. Highly conserved predicted binding sites and the mutant sites are shown in Fig. 4A in the 3'-UTR of TMED5. EGFP reporter assay indicated that the EGFP activity of TMED5 was decreased by miR-433 overexpression and increased by miR-433 knockdown in A549 and H1299 cells, indicating that miR-433 directly targeted TMED5 (Fig. 4B). In addition, altered miR-433 failed to affect the EGFP intensity of the plasmid carrying TMED5 3'-UTR MUT in A549 and H1299 cells (Fig. 4C). Moreover, TMED5 mRNA and protein expression was decreased by miR-433 overexpression and enhanced by miR-433-knockdown in A549 and H1299 cells (Fig. 4D and E). The protein expression levels of TMED5 were markedly increased in NSCLC tissues compared with in adjacent normal tissues using the GEPIA database (Fig. 4F). The mRNA expression levels of TMED5 were also markedly increased in NSCLC tissues according to TCGA database, especially in chemotherapy-resistant NSCLC tissues (Fig. 4G). In addition, patients with NSCLC with high TMED5 expression exhibited a poor prognosis according to The Human Protein Atlas (Fig. 4H).

TMED5 functions as an oncogene in NSCLC. The plasmid of TMED5 overexpression (pTMED5) was transfected into NSCLC cells. pTMED5 transfection enhanced TMED5 mRNA and protein expression in A549 and H1299 cells (Fig. 5A and B). CCK-8 assay revealed that pTMED5 promoted cell viability in A549 and H1299 cells (Fig. 5C). Colony formation assay indicated that pTMED5 induced a significant increase in colony formation in A549 and H1299 cells (Fig. 5D). Additionally, pTMED5 accelerated G_1 to S and G_2 transition in NSCLC cells (Figs. 5E and F, and S2A and B). Transfected pTMED5 significantly decreased the apoptotic rate (Figs. 5G and S2C), as well as decreased the levels of cleaved caspase 3 and cleaved PARP in NSCLC cells (Fig. 5H). Cisplatin chemoresistance was increased in A549 and H1299 cells treated with pTMED5 than that in cells transduced with pcDNA3 in a dose-dependent manner with 0-4 μg/ml cisplatin, as assessed by CCK-8 assay (Fig. 5I). In addition, TMED5-overexpressing A549 and H1299 cells repaired DNA breaks more quickly than control vector-treated cells (Fig. 5J). TMED5 overexpression inhibited the protein expression levels of 53BP1 and H2AX in A549 and H1299 cells (Fig. 5K). Furthermore, deep single cell transcriptome data in NSCLC tissues revealed upregulated TMED5 expression in the subset of CD4-CD69 (Non-traditional regulatory T cells), CD4-CXCL13 (exhausted

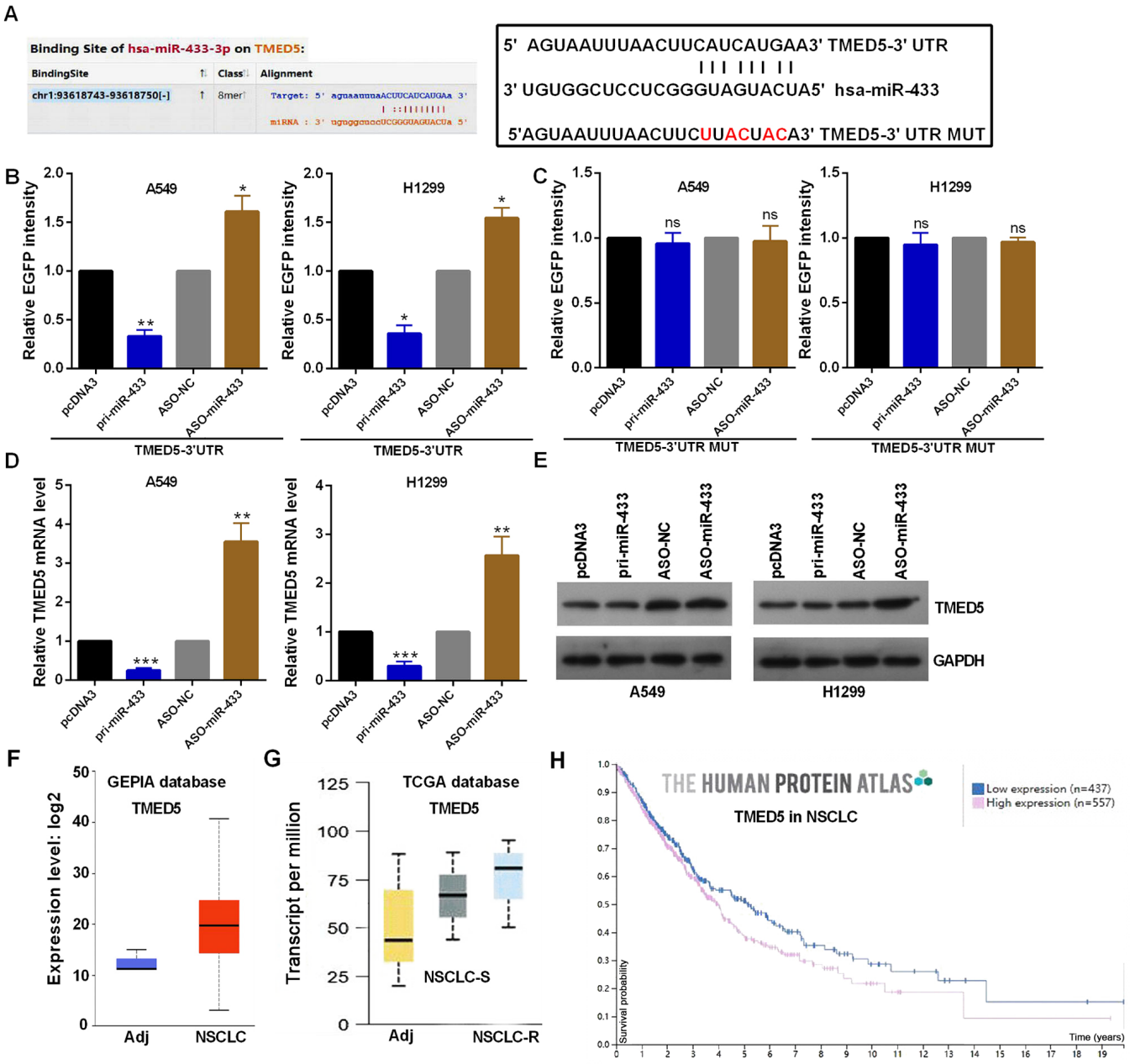

Figure 4. miR-433 directly targets TMED5. (A) Predicted miR-433 binding sites in TMED5 mRNA WT and MUT using StarBase V3.0. (B and C) EGFP intensity in A549 and H1299 cells co-transfected with pri-miR-433 or ASO-miR-433 and the WT or MUT 3'-UTR of TMED5. (D) TMED5 mRNA expression with the indicated transfections was measured by reverse transcription-quantitative PCR assay in A549 and H1299 cells. (E) TMED5 protein expression in A549 and H1299 cells transfected with pri-miR-433 or ASO-miR-433 and respective controls was determined by western blotting. (F) GEPIA database showing the TMED5 protein expression. (G)TCGA database showing the TMED5 mRNA expression. (H) Human Protein Atlas showing that high protein expression levels of TMED5 predicted a poor prognosis in patients with NSCLC. *P<0.05, **P<0.01 and ***P<0.001 vs. pcDNA3 or ASO-NC. ns, not significant; WT, wild-type; MUT, mutated; 3'-UTR, 3'-untranslated region; miR, microRNA; TMED5, transmembrane p24 trafficking protein 5; NC, negative control; ASO, antisense oligonucleotide; TCGA, The Cancer Genome Atlas; NSCLC, non-small cell lung cancer; R, resistant; Adj, adjacent.

CD4 T cells), CD4-CTLA4 (naïve CD4 T cells and Treg cells), CD8-ZNF683 (pre-exhaustion CD8 T cells) and CD8-LAYN (exhausted CD8^{+} T cells) compared with the normal tissues, indicating that CD69, CXCL13, CTLA4, ZNF683 and LAYN may be negative regulatory genes in cellular immune response (Fig. 5L and M).

miR-433 regulates the WNT/β-catenin signaling pathway through TMED5. As shown in Fig. 6A, TMED5 overexpression markedly promoted the phosphorylation of β-catenin (p-β-catenin), but not total β-catenin expression, as well as significantly increased c-myc and cyclin D1 expression. miR-433 overexpression in A549 and H1299 cells co-transfected with pTMED5 blocked the TMED5-induced increases of protein expression levels, including those of p-β-catenin, c-myc and cyclin D1 (Fig. 6A). Additionally, TOP/FOP luciferase reporter assays identified that miR-433 overexpression significantly inhibited the Top/Fop radio, indicating the inactivation of the WNT signaling pathway by miR-433 overexpression in A549 and H1299 cells (Fig. 6B).

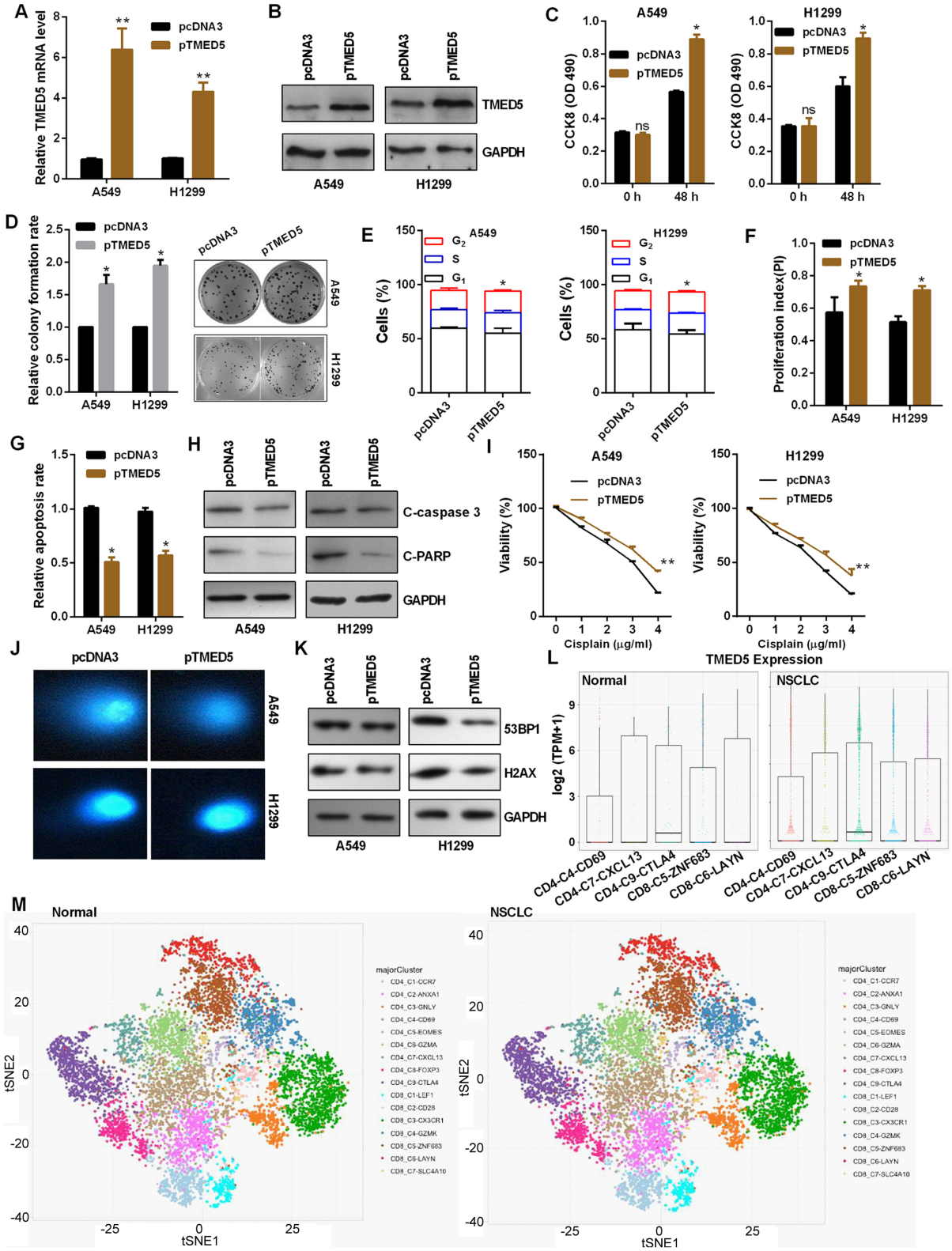

Figure 5. TMED5 functions as an oncogene in NSCLC. Efficiency of pTMED5 was detected by (A) reverse transcription-quantitative PCR and (B) western blot assay in A549 and H1299 cells. (C) Role of altered TMED5 expression on the viability of A549 and H1299 cells was detected by CCK-8 assay. (D) Colony formation assay showed the proliferation ability of A549 and H1299 cells transfected with pTMED5. (E) Flow cytometric analysis showed that TMED5 overexpression in A549 and H1299 cells resulted in a decrease of cells in the G_0/G_1 phase and an increase of cells in the S and G_2 phases. (F) TMED5 overexpression promoted the proliferation index. (G) Flow cytometric assay showed that TMED5 overexpression decreased apoptosis in A549 and H1299 cells. (H) Western blotting showed the protein expression levels of C-caspase 3 and C-PARP in A549 and H1299 cells. (I) Transfected A549 and H1299 cells were treated with 0-4 μg/ml cisplatin in 96-well plates for 24 h. CCK-8 assay was then used to investigate cell viability. (J) Comet assays showed the degree of DNA breaks in A549 and H1299 cells transfected with the indicated plasmids treated with 10 μg/ml taxol for 4 h. (K) Western blotting showed the protein expression levels of 53BP1 and H2AX in A549 and H1299 cells transfected with the indicated plasmids treated with 10 μg/ml taxol for 4 h. (L and M) Deep single cell transcriptome data showed the immune cell infiltration in NSCLC and the control group. These figures were taken form 'Global characterization of T cells in non-small cell lung cancer by single-cell sequencing' (http://lung.cancer-pku.cn/index.php). *P<0.05 and **P<0.01 vs. pcDNA3. ns, not significant; p, plasmid; CCK-8, Cell Counting Kit-8; OD, optical density; C, cleaved; PARP, poly(ADP-ribose)polymerase; 53BP1, tumor protein p53 binding protein 1; NSCLC, non-small cell lung cancer; TMED5, transmembrane p24 trafficking protein 5; TPM, transcript per million.

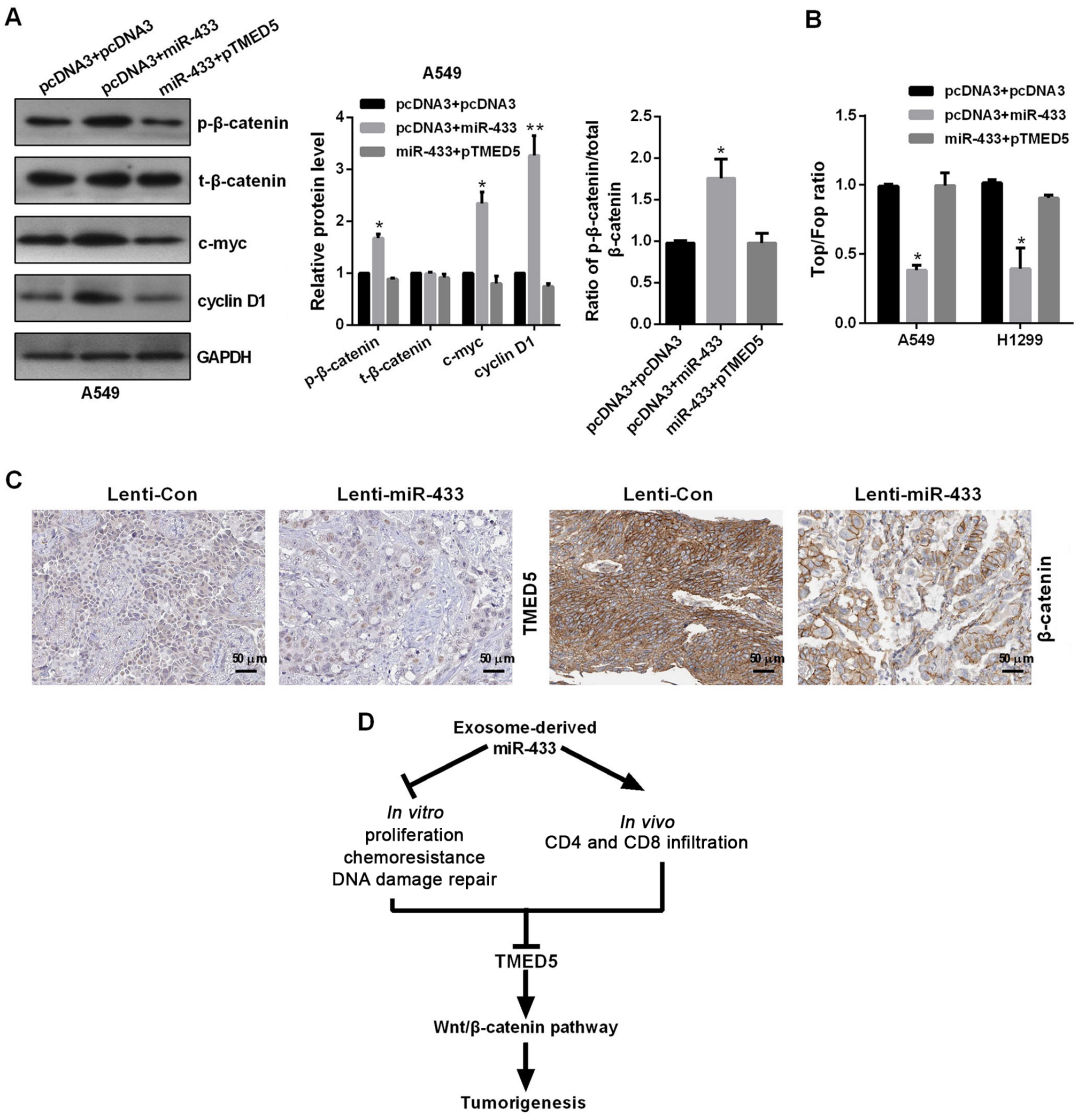

Figure 6. miR-433 inhibits the WNT signaling pathway through TMED5. (A) Western blotting showed the protein levels of p-β-catenin, β-catenin, c-myc, cyclin D1 and GAPDH in A549 and H1299 cells transfected with the indicated plasmids. (B) Top/Fop luciferase reporter assay was performed to detect WNT activity. (C) Immunohistochemistry showed the protein expression levels of TMED5 and β-catenin. Scale bar, 50 μm. (D) Model of potential association of miR-433 and its target gene TMED5. *P<0.05 and **P<0.01 vs. pcDNA3 + pcDNA3. p, plasmid; TMED5, transmembrane p24 trafficking protein 5; miR, microRNA; p, phosphorylated; t, total; Lenti, lentivirusl Con, control.

Finally, IHC was performed to detect the expression levels of TMED5 and β-catenin in miR-433-mediated tumors *in vivo*. The results revealed that Lenti-miR-433 inhibited the protein expression levels of TMED5 and β-catenin (Fig. 6C).

Discussion

Emerging evidence has identified that miRNAs serve crucial roles in various biological functions, such as differentiation, proliferation, chemotherapy resistance, metastasis, autophagy and DNA damage, in a number of diseases, including intervertebral disc degeneration, Alzheimer's disease and Huntington's disease (25). Differentially expressed miRNAs are closely associated with tumors and the tumor microenvironment (25,26). Furthermore, exosomal miRNAs released by cancer cells can directly induce a series of phenotypes. For example, exosomal miR-766-3p promotes cell migration and invasion through homeobox A13 in ESCC (27). Exosomal miR-500a-3p promotes cisplatin resistance and stemness via negatively regulating FBXW7 in gastric cancer (28). In ovarian cancer, high miR-433-expressing cells release miR-433 into the growth media via exosomes, which in turn can induce a senescence bystander effect (29). The present study reported that exosomal miR-433 expression was lower in plasma of patients with chemotherapy-resistant NSCLC compared with in plasma of patients with chemotherapy-sensitive NSCLC and in normal serum, and miR-433 expression was significantly negatively associated large tumor size, advanced TNM stage, distant metastasis and a poor prognosis in patients with NSCLC. Notably, Weng *et al* (30) also reported that PCGEM1 prostate-specific transcript (PCGEM1) was highly expressed in NSCLC cells, while miR-433-3p was lowly expressed in NSCLC cells. PCGEM1 silencing or miR-433-3p overexpression inhibit cell proliferation, migration and invasion, but accelerate apoptosis in NSCLC cells (30).

The tumor microenvironment (TME) represents a key factor for tumor heterogeneity maintenance, tumor progression and drug resistance, and is composed of different cellular populations, such as stromal, immune, endothelial and cancer stem cells (31). Exosomal miRNAs from tumor cells disturb T-cell metabolism and immune response, and increase the production of cytokines in the TME (32). miRNAs in exosomes promote Treg expansion accompanying ERK, STAT1 and STAT3 expression, but inhibit the differentiation of T helper (Th)1 and Th17 cells, as well as leading to an amplification of cytokine production in the TME (33). The present study reported that exosomal miR-433 inhibited tumor growth *in vitro* and *in vivo* by blocking the cell cycle and promoting apoptosis and CD4 and CD8 T-cell infiltration. However, the underlying mechanism requires further investigation. Exosomal miR-433 also inhibited chemoresistance to cisplatin by regulating DNA damage.

The Wnt signaling pathway is one of the most important signaling pathways during development of a number of tumors and other diseases, including embryonic development and maturation of the central nervous system (34,35). Increasing evidence has indicated miRNA dysregulation and the Wnt/β-catenin signaling pathway jointly drive carcinogenesis, cancer metastasis and drug-resistance (36-40). The present study reported that miR-433 inactivated the Wnt/β-catenin signaling pathway by targeting TMED5 in NSCLC.

In conclusion, the findings of the present study provide novel insight into the role of tumor-derived exosomal miR-433 in NSCLC progression (Fig. 6D). NSCLC-derived exosomal miR-433 may mediate cell proliferation, tumor growth, cell cycle, apoptosis, chemoresistance and CD4 and CD8 T-cell infiltration, which may be associated with the enrichment of exosomal miR-433 targeting the downregulation of TMED5 and the WNT/β-catenin signaling pathway. Therefore, based on the current findings, targeting exosomes and exosomal miRNAs may be used as an effective anticancer strategy.

Acknowledgements

The authors would like to thank Dr Shujuan Yuan (Tianjin Medical University, Tianjin, China) for her effort with the revision of the language of the manuscript.

Funding

No funding was received.

Availability of data and materials

The datasets used and/or analyzed during the current study are available from the corresponding author on reasonable request.

Authors' contributions

RH conceived and designed the current study, and contributed to writing the manuscript. RH and BL performed the experiments and confirm the authenticity of all the raw data. RZ and YZ analyzed and interpreted the data. All authors read and approved the final manuscript.

Ethics approval and consent to participate

The current study was conducted under the International Ethical Guidelines for Biomedical Research Involving Human Subjects with the approval of the Ethics Committee of Tianjin Medical University Cancer Institute and Hospital and performed in accordance with the Declaration of Helsinki (approval no. EK2019034), and all participants provided their written informed consent. The animal experiments were approved by the Institutional Animal Care and Use Committee of Tianjin Medical University Cancer Institute and Hospital (approval no. LLSP2019017).

Patient consent for publication

Not applicable.

Competing interests

The authors declare that they have no competing interests.

References

1. Nasim F, Sabath BF and Eapen GA: Lung cancer. Med Clin North Am 103: 463-473, 2019.
2. Duma N, Santana-Davila R and Molina JR: Non-small cell lung cancer: Epidemiology, screening, diagnosis, and treatment. Mayo Clin Proc 94: 1623-1640, 2019.
3. Hoy H, Lynch T and Beck M: Surgical treatment of lung cancer. Crit Care Nurs Clin North Am 31: 303-313, 2019.
4. Skoulidis F and Heymach JV: Co-occurring genomic alterations in non-small-cell lung cancer biology and therapy. Nat Rev Cancer 19: 495-509, 2019.
5. Yoneda K, Imanishi N, Ichiki Y and Tanaka F: Immune checkpoint inhibitors (ICIs) in non-small cell lung cancer (NSCLC). J UOEH 40: 173-189, 2018.
6. Xie Y, Dang W, Zhang S, Yue W, Yang L, Zhai X, Yan Q and Lu J: The role of exosomal noncoding RNAs in cancer. Mol Cancer 18: 37, 2019.
7. Hu C, Meiners S, Lukas C, Stathopoulos GT and Chen J: Role of exosomal microRNAs in lung cancer biology and clinical applications. Cell Prolif 53: e12828, 2020.
8. Williams M, Cheng YY, Blenkiron C and Reid G: Exploring mechanisms of microRNA downregulation in cancer. Microrna 6: 2-16, 2017.
9. Deng S, Calin GA, Croce CM, Coukos G and Zhang L: Mechanisms of microRNA deregulation in human cancer. Cell Cycle 7: 2643-2646, 2008.
10. Rupaimoole R, Calin GA, Lopez-Berestein G and Sood AK: miRNA deregulation in cancer cells and the tumor microenvironment. Cancer Discov 6: 235-246, 2016.
11. Calin GA and Croce CM: MicroRNA signatures in human cancers. Nat Rev Cancer 6: 857-866, 2006.
12. Svoronos AA, Engelman DM and Slack FJ: OncomiR or tumor suppressor? The duplicity of microRNAs in cancer. Cancer Res 76: 3666-3670, 2016.
13. Han F, Huang D, Huang X, Wang W, Yang S and Chen S: Exosomal microRNA-26b-5p down-regulates ATF2 to enhance radiosensitivity of lung adenocarcinoma cells. J Cell Mol Med 24: 7730-7742, 2020.
14. Wang HX, Wang XY, Fei JW, Li FH, Han J and Qin X: MicroRNA-23B inhibits non-small cell lung cancer proliferation, invasion and migration via downregulation of RUNX2 and inhibition of Wnt/B-catenin signaling pathway. J Biol Regul Homeost Agents 34: 825-835, 2020.
15. Qu Y, Zhu J, Liu J and Qi L: Circular RNA circ_0079593 indicates a poor prognosis and facilitates cell growth and invasion by sponging miR-182 and miR-433 in glioma. J Cell Biochem 120: 18005-18013, 2019.
16. Ding L and Zhang H: Circ-ATP8A2 promotes cell proliferation and invasion as a ceRNA to target EGFR by sponging miR-433 in cervical cancer. Gene 705: 103-108, 2019.

17. Yan L, You WQ, Sheng NQ, Gong JF, Hu LD, Tan GW, Chen HQ and Wang ZG: A CREB1/miR-433 reciprocal feedback loop modulates proliferation and metastasis in colorectal cancer. Aging (Albany NY) 10: 3774-3793, 2018.
18. Zhang T, Jiang K, Zhu X, Zhao G, Wu H, Deng G and Qiu C: miR-433 inhibits breast cancer cell growth via the MAPK signaling pathway by targeting Rap1a. Int J Biol Sci 14: 622-632, 2018.
19. Shi Q, Wang Y, Mu Y, Wang X and Fan Q: miR-433-3p inhibits proliferation and invasion of esophageal squamous cell carcinoma by targeting GRB2. Cell Physiol Biochem 46: 2187-2196, 2018.
20. Wang YJ, Zhang ZF, Fan SH, Zhuang J, Shan Q, Han XR, Wen X, Li MQ, Hu B, Sun CH, *et al*: MicroRNA-433 inhibits oral squamous cell carcinoma cells by targeting FAK. Oncotarget 8: 100227-100241, 2017.
21. Liu N, Liu Z, Zhang W, Li Y, Cao J, Yang H and Li X: MicroRNA-433 reduces cell proliferation and invasion in non-small cell lung cancer via directly targeting E2F transcription factor 3. Mol Med Rep 18: 1155-1164, 2018.
22. Li J, Chen M and Yu B: miR-433 suppresses tumor progression via Smad2 in non-small cell lung cancer. Pathol Res Pract 215: 152591, 2019.
23. Livak KJ and Schmittgen TD: Analysis of relative gene expression data using real-time quantitative PCR and the 2(-Delta Delta C(T)) method. Methods 25: 402-408, 2001.
24. Yang Z, Sun Q, Guo J, Wang S, Song G, Liu W, Liu M and Tang H: GRSF1-mediated MIR-G-1 promotes malignant behavior and nuclear autophagy by directly upregulating TMED5 and LMNB1 in cervical cancer cells. Autophagy 4: 668-685, 2019.
25. Vishnoi A and Rani S: miRNA biogenesis and regulation of diseases: An overview. Methods Mol Biol 1509: 1-10, 2017.
26. Sandiford OA, Moore CA, Du J, Boulad M, Gergues M, Eltouky H and Rameshwar P: Human aging and cancer: Role of miRNA in tumor microenvironment. Adv Exp Med Biol 1056: 137-152, 2018.
27. Liu S, Lin Z, Zheng Z, Rao W, Lin Y, Chen H, Xie Q, Chen Y and Hu Z: Serum exsomal miR-766-3p expression is associated with poor prognosis of esophageal squamous cell carcinoma. Cancer Sci 110: 3881-3892, 2020.
28. Lin H, Zhang L, Zhang C and Liu P: Exosomal miR-500a-3p promotes cisplatin resistance and stemness via negatively regulating FBXW7 in gastric cancer. J Cell Mol Med 24: 8930-8941, 2020.
29. Weiner-Gorzel K, Dempsey E, Milewska M, McGoldrick A, Toh V, Walsh A, Lindsay S, Gubbins L, Cannon A, Sharpe D, *et al*: Overexpression of the microRNA miR-433 promotes resistance to paclitaxel through the induction of cellular senescence in ovarian cancer cells. Cancer Med 4: 745-758, 2015.
30. Weng L, Qiu K, Gao W, Shi C and Shu F: LncRNA PCGEM1 accelerates non-small cell lung cancer progression via sponging miR-433-3p to upregulate WTAP. BMC Pulm Med 20: 213, 2020.
31. Santos P and Almeida F: Role of exosomal miRNAs and the tumor microenvironment in drug resistance. Cells 9: 1450, 2020.
32. Bland CL, Byrne-Hoffman CN, Fernandez A, Rellick SL, Deng W and Klinke DJ 2nd: Exosomes derived from B16F0 melanoma cells alter the transcriptome of cytotoxic T cells that impacts mitochondrial respiration. FEBS J 285: 1033-1050, 2018.
33. Ye SB, Li ZL, Luo DH, Huang BJ, Chen YS, Zhang XS, Cui J, Zeng YX and Li J: Tumor-derived exosomes promote tumor progression and T-cell dysfunction through the regulation of enriched exosomal microRNAs in human nasopharyngeal carcinoma. Oncotarget 5: 5439-5452, 2014.
34. Taciak B, Pruszynska I, Kiraga L, Bialasek M and Krol M: Wnt signaling pathway in development and cancer. J Physiol Pharmacol 69: 185-196, 2018.
35. Kassumeh S, Weber GR, Nobl M, Priglinger SG and Ohlmann A: The neuroprotective role of Wnt signaling in the retina. Neural Regen Res 16: 1524-1528, 2021.
36. Stewart DJ: Wnt signaling pathway in non-small cell lung cancer. J Natl Cancer Inst 106: djt356, 2014.
37. Tang J, Gao W, Liu G, Sheng W, Zhou J, Dong Q and Dong M: miR-944 suppresses EGF-induced EMT in colorectal cancer cells by directly targeting GATA6. Onco Targets Ther 14: 2311-2325, 2021.
38. Wu Z, Zhang Y, Yang Z, Zhu Y, Xie Y, Zhou F and Cai L: Elevation of miR-302b prevents multiple myeloma cell growth and bone destruction by blocking DKK1 secretion. Cancer Cell Int 21: 187, 2021.
39. Xie Y, Xue C, Guo S and Yang L: MicroRNA-520a suppresses pathogenesis and progression of non-small-cell lung cancer through targeting the RRM2/Wnt axis. Anal Cell Pathol (Amst) 2021: 9652420, 2021.
40. Wang H, Yang Q, Li J, Chen W, Jin X and Wang Y: MicroRNA-15a-5p inhibits endometrial carcinoma proliferation, invasion and migration via downregulation of VEGFA and inhibition of the Wnt/β-catenin signaling pathway. Oncol Lett 21: 310, 2021.